ELSEVIER

Polymer 41 (2000) 6237–6249

polymer

Melting and heat capacity of gel-spun, ultra-high molar mass polyethylene fibers☆

Y.K. Kwon[a,b], A. Boller[a,b], M. Pyda[a,b], B. Wunderlich[a,b,*]

[a]*Department of Chemistry, The University of Tennessee, Knoxville, TN 37996-1600, USA*
[b]*Chemical and Analytical Sciences Division, Oak Ridge National Laboratory, Oak Ridge, TN 37831-6197, USA*

Received 6 August 1999; received in revised form 5 November 1999; accepted 9 November 1999

Abstract

The melting behaviors of gel-spun, ultra-high molar mass polyethylene fibers have been investigated using standard differential scanning calorimetry and wide-angle X-ray diffraction. For laterally constrained fibers the standard DSC exhibits the usually reported two melting peaks (one at about 415 K and one at about 423 K), a glass transition (at about 275 K) and an unusually large and reversible heat capacity as one approaches the melting peaks (starting at about 350–370 K). Earlier observations that sometimes only the lower melting endotherm is retained, are proven to be of fibers free of longitudinal *and* lateral constraints. Up to the beginning of major melting, all fibers are mainly orthorhombic. The orthorhombic–hexagonal transition is proven to occur only for the constrained fibers, implying that the hexagonal phase is a non-equilibrium phase, usually not present in the initial fibers. An oriented, intermediate phase, discovered by solid state NMR and full-pattern X-ray analysis, gives rise to a substantially broadened glass transition that reaches to about 300 K, compared to the glass transition of the amorphous polyethylene with a midpoint at 237 K and end at 250 K. Published by Elsevier Science Ltd.

Keywords: Ultra-high molar mass polyethylene; Melting; Orthorhombic–hexagonal transition

1. Introduction

The structure and physical properties of ultra-high molar mass polyethylene (UHMM-PE) fibers have been widely investigated [1–14]. In our previous study, the structures of a series of UHMM-PE fibers were analyzed with full-pattern X-ray diffraction [9], small angle X-ray scattering (SAXS) [9], solid state ^{13}C nuclear magnetic resonance (^{13}C NMR) [10,13,14], differential scanning calorimetry (DSC) [11], thermomechanical analysis (TMA) [12] and optical microscopy [9,12]. It was reported that these fibers consist of three phases, the crystalline, oriented-intermediate, and amorphous phases, at room temperature. The crystalline phase was mainly orthorhombic, along with a small amount of monoclinic crystals [9]. The chains of the intermediate phase consist of mobile, non-crystalline chains with mostly *trans*-conformations that are aligned, preferentially parallel, to the fiber axis, but are disordered laterally [9,10,13,14]. These fibers keep their three-phase structure over a wide temperature and pressure range. Because polyethylene can be considered a one-component material, this violates the phase rule and, thus, the sample must be in a non-equilibrium, metastable state [15].

Owing to the metastability of the multi-phase, semi-crystalline polymer, a series of thermal events can take place prior to melting and during the melting transition itself. These effects start with the glass transition that is usually broadened in semicrystalline polymers and may, in the present case, have a separate component from the mobile, intermediate phase. Small crystals may melt at less than the equilibrium melting temperature [16]. Recrystallization or reorganization into more stable crystals of the same or different polymorphs can occur. Melting into a strained rather than an isotropic melt results in an increase of the observed melting temperature. Because of the variety of fibers available and the many possible effects, conflicting reports and interpretation of the thermal properties were published in the past.

Double melting peaks are common in polymers [16]. For the discussion of the melting of polyethylene fibers, it is necessary to remember that equilibrium melting of orthorhombic, extended chain crystals [17] occurs sharply at

* Corresponding author. Tel.: +1-865-974-0652; fax: +1-865-974-3419. Corresponding address. The University of Tennessee, Department of Chemistry, Knoxville, TN 37996-1600, USA.

0032-3861/00/$ - see front matter Published by Elsevier Science Ltd.
PII: S0032-3861(99)00839-3

Table 1
Properties of UHMM PE fibers

Sample	Modulus (GPa)[a]	Tensile strength (GPa)[a]	Density (mg/m^3)	Crystallinity (%)[b]
PE-I	179	3.9	0.964	(80) (84) [≈ 67]
PE-II	–	–	0.971	(84) (83)
PE-III	125	2.7	0.974	(86) (92)
PE-IV	59	1.6	0.978	(88) (77) [≈ 52]

[a] Provided by Allied-Signal Inc.
[b] First value from density, second, from calorimetry and third, from heat capacity at 300 K (30 and 38% intermediate phase for PE-I and IV, respectively, see Fig. 10).

414.6 K [18]. This melting point results also from theoretical considerations, by extrapolation of the equilibrium melting temperatures of paraffins, consideration of the temperature dependence of the thermodynamic parameters [18–20] and the extrapolation of zero-entropy production melting points of lamellar crystals to infinite thickness [16]. Higher melting temperatures may arise from faster heating than the melting kinetics permits (superheating) or by local melting equilibria with strained melts [16]. In the case of the UHMM-PE fibers, double endotherms are frequently observed and were assigned an orthorhombic–hexagonal phase transition for the low-temperature endotherm and a complete isotropization for the high-temperature endotherm [21,22]. Alternatively, it was suggested that the lower-melting component is because of melting of thin, lamellar crystals, while the higher one is caused by thicker lamellae or extended-chain crystals [23]. Bastiaansen and Lemstra [24], however, reported that the onset temperature of unconstrained melting of chopped fibers of UHMM-PE was at 415 K with only one melting peak. Pennings and Zwijnenburg [22] demonstrated that the same fibers, when constrained to constant length, show three and even four endothermic peaks. In our previous study, we investigated the multiple melting peaks of UHMM-PE fibers by varying the sample size, the manner of packing of the individual fibers and by introducing inert media to enhance heat transport [9,11,12]. Both, the placement of single layers of fibers at the bottom of the pan and the filling of the spaces between the fibers with powdered alumina made the multiple melting peaks disappear. The effects of sample mass and arrangement inside the pan suggested, that the multiple melting peaks of UHMM-PE fibers is linked to sample size, shrinkage and thermal conductivity within the sample pan.

External restraints on fibers are known to retard the stress-release within the sample and hinder the melted molecules to reach full isotropization. As a result, the melting temperature increases [16,25]. It leads to a lesser gain of entropy on fusion, which causes the higher melting temperature. Another reason for an increase in melting temperature is the annealing or reorganization of fibers during heating. This was proven by chemical crosslinking of the amorphous regions so that the less mobile chains cannot be drawn into the crystals, as is needed for crystal reorganization [16,26].

In the present study we have extended the full thermodynamic characterization of polyethylene to the gel-spun fibers. The glass transition is detailed, and for the first time we can supply some experimental evidence that the intermediate phase has a sizeable latent heat on melting. To resolve the conflicting reports in the literature of single and double peak melting of the UHMM gel-spun-PE fibers, we use a series of standard DSC experiments and temperature-resolved wide-angle X-ray diffraction techniques. The key point is that the fibers must be free of constraints to completely melt with a single peak at the low melting temperature. In DSC experiments the lateral constraint, introduced by sealing the sample pan, will be shown to be sufficient to hinder shrinkage of the fibers, which are extended by as much as 100 times their original length. This simple observation accounts for the frequent observation of multiple melting peaks by DSC.

In the DSC measurement, samples of different sizes were used to separate instrumental effects from sample effects. For the study of the melting characteristics we used a power-compensating type DSC, which has sample and reference calorimeters located in close proximity to their temperature sensors and therefore a short path for heat conduction [27,28]. To measure the effect of gel spinning on heat capacity, a heat-flux DSC was used with larger sample masses, in order to increase the precision of the measurement and to allow an observation of possible changes in the glass transition.

2. Experimental

2.1. Materials

The heat capacity study included four gel-spun fibers. All of the UHMM-PE fibers were provided by Allied-Signal Inc., and had similar high molar masses ($M_W > 10^6$ Da). Two of them (PE-I and PE-IV) were research samples made from the same base polymer, but with different processing conditions (sample IV was not hot stretched after spinning). The other two were commercial Spectra™ 2000 and 900 fibers (PE-II and PE-III, respectively). All fibers were prepared by gel-spinning [29–31] and were the same as used in our prior research [9–14]. The time-resolved X-ray

Table 2
Heat capacities of the fibers (J K^{-1} mol^{-1})

T (K)	PE-I	PE-II	PE-III	PE-IV
175	14.25	14.32	14.18	14.27
180	14.75	14.75	14.75	14.75
185	14.98	15.08	15.07	15.07
190	15.46	15.50	15.46	15.46
195	15.57	15.76	15.60	15.69
200	16.06	16.16	16.11	16.18
205	16.27	16.43	16.33	16.39
210	16.79	16.80	16.69	16.81
215	16.96	17.13	16.94	17.07
220	17.46	17.50	17.35	17.55
225	17.67	17.72	17.69	17.81
230	18.19	18.12	18.07	18.30
235	18.40	18.47	18.36	18.57
240	18.93	18.94	18.86	19.06
245	19.15	19.23	19.18	19.47
250	19.73	19.73	19.58	19.94
255	20.00	20.18	19.93	20.27
260	20.56	20.60	20.43	20.88
265	20.86	20.93	20.84	21.30
270	21.46	21.52	21.26	21.89
275	21.77	21.93	21.55	22.40
280	22.28	22.45	21.98	23.09
285	22.52	22.79	22.42	23.70
290	23.13	23.27	22.92	24.34
295	23.37	23.64	23.26	24.85
300	23.95	24.12	23.79	25.43
305	24.19	24.34	24.22	25.69
310	24.84	24.86	24.76	26.22
315	25.22	25.35	25.24	26.68
320	25.73	25.85	25.69	27.31
325	26.04	26.21	26.15	27.72
330	26.67	26.79	26.76	28.32
335	27.17	27.30	27.19	28.86
340	27.74	27.87	27.72	29.61
345	28.18	28.43	28.39	30.24
350	28.90	29.11	28.99	30.92
355	29.44	29.61	29.60	31.62
360	30.12	30.38	30.33	32.46
365	30.84	31.05	31.10	33.45
370	31.57	31.86	31.84	34.29
375	32.62	32.77	32.84	35.90
380	33.49	33.75	33.77	37.08
385	34.89	35.03	35.16	39.54
390	36.04	36.17	36.32	40.35

analysis and the melting peak study were carried out with as delivered bundles of PE-III (Spectra 900™). Density, crystallinity and mechanical properties of the samples are summarized in Table 1.

2.2. Heat-flux calorimetry

A commercial Mettler-Toledo heat-flux DSC820 module was used for the measurement of heat capacity [12,32]. Dry nitrogen gas with a flow rate of 10 ml min^{-1} was purged through the cell. The samples for the temperature calibration were indium (429.7 K), naphthalene (353.42 K), *n*-octane (116.4 K), acetone (177.9 K), cyclohexane s/s (186.09 K), cyclohexane s/1 (297.7 K), cycloheptane (265.1 K) and tin (505.05 K). The onset of melting was determined by extrapolation of the melting peak to the baseline. In order to achieve maximum sample size for heat capacity measurements, the PE fibers were wound onto a spool and pushed after winding into the sample pan [12]. The sample masses were in the order of 16–30 mg, depending on the individual fiber properties.

The error in the heat capacity calculation is estimated to be about 1% above 300 K and 3% below 200 K [12]. All sample placements were done with the auto-sampler for increased repeatability. For the heat capacity determination, the range from 173 to 403 K was used in order to avoid problems associated with shrinkage in the calorimeter pan when approaching the melting temperature. The measurements were started with an isotherm of 5 min at 173 K. The temperature range from the start temperature to 303 K was then subdivided into steps of 20 K. Each of the steps was measured with a heating rate of 10 K min^{-1}. The time for equilibration at each isothermal temperature was 1 min. The final isotherm at 393 K was again extended to 5 min. This heating run was followed with a cooling ramp, covering the same isothermal temperatures. A second overall heating ramp was started next at 183 K. In this way, the approach to the steady state of the individual segments was shifted from the first to the second overall heating ramp. A second overall cooling segment concluded the experiment. For each sample, at least six of these experiments were performed and averaged. Sample, empty-pan and sapphire measurements were performed with the same temperature programs in order to evaluate the heat capacities [33]. Special care was taken to match sample pans, leaving the same pan on the reference position. The sample pans for all heat capacity measurements weighed 49.05 ± 0.02 mg. The same instrumentation was also used for a first assessment of the melting peaks of the gel-spun fibers as was reported earlier [11,12].

2.3. Power compensation calorimetry

The melting behaviors of the UHMM-PE fibers PE-III were made with a power-compensation DSC of the types: Perkin–Elmer PYRIS-1 with a liquid nitrogen accessory and Perkin–Elmer DSC 7 with a mechanical refrigeration accessory. The measurements were extended from sufficiently low temperature to connect to the vibrational heat capacity of the fibers and extended into the melt. During measurements, dry nitrogen gas was allowed to flow through the DSC cell at 20 ml min^{-1}. The temperature signal was calibrated by the onset of melting of indium and cyclohexanone at a heating rate of 10 K min^{-1}. The heat-flow rate was calibrated with the heat of fusion of indium.

The melting behavior of UHMM-PE fibers was measured as follows. The cut fibers, with a length of approximately 0.5 mm, were placed parallel in the aluminum pan. These fibers were analyzed under two conditions: in one case, the fibers were free to retract during heating; and in the other,

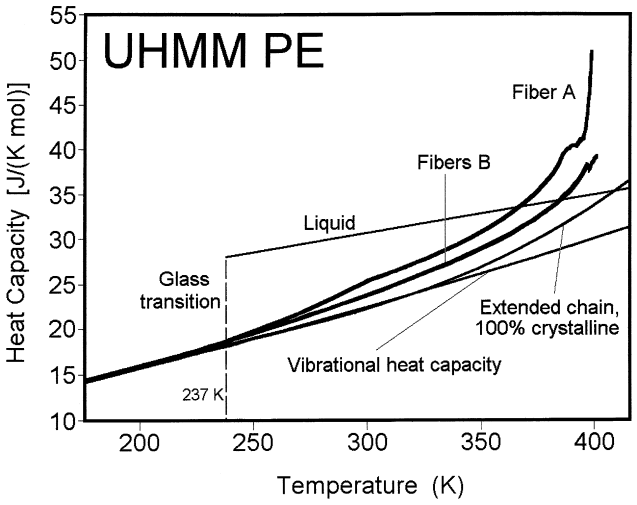

Fig. 1. Comparison of the heat capacities of UHMM-PE fibers with ATHAS data bank data for the liquid polymer, the vibrational heat capacity of the solid and experimental data for close to 100% crystalline, extended chain polyethylene. Fiber A: sample PE-IV. Fiber B: samples PE-I to III.

they were hindered in their shrinking by crimping a lid tightly onto the pan. Sample masses varied from 25 μg to 1.2 mg. In order to achieve statistically significant averages, a series of heating and cooling scans with a rate of 10 K min^{-1} was carried out at least five times for each experiment.

2.4. X-ray diffraction

Temperature-dependent equatorial and meridional wide-angle X-ray diffraction data were collected on a bundle of PE-III fibers. For measurement under constraint, the fibers were wound tightly around a support in the externally heated hot stage. Data measured without constraint were also carried out earlier and were published as Fig. 3 in Ref. [9].

The fibers were always aligned perpendicular to the direction of the X-ray beam. The intensity measurements were gathered using a reflected X-ray beam on a PAD-X diffractometer of Scintac Inc. The X-rays were CuK_α radiations ($\lambda = 1.518$ Å) and had a Zr filter placed on the incident beam with electronic discrimination at the solid-state detector. Intensities were measured within the range of scattering angles (2θ) of 5–40° and 60–80° in the equatorial and meridional directions, respectively.

The integral half-widths of the diffracted intensities were measured to determine their transverse crystallite sizes and assessed using the Scherrer equation [34]. To get a quantitative value, these widths need to be corrected for the width of the primary beam. Using an Si standard, provided by Phillips Co., the instrumental broadening was estimated in the range of $10 \leq 2\theta \leq 30°$.

3. Results

3.1. Heat capacity

The results of the heat capacity measurements for samples PE-I to IV are listed in Table 2. They fall clearly into two groups, sample PE-IV (Fiber A), the sample that was not hot-stretched after spinning, and samples I to III (Fiber B). To eliminate minor systematic errors, all heat capacities were shifted to agree with the vibration-only heat capacity at 180 K, a temperature where only negligible deviations between the samples are expected. Fig. 1 shows the so-corrected data. For comparison, the ATHAS Data Bank values are given for the heat capacities of the liquid, which includes large-amplitude motion (conformational changes) and the vibrational heat capacity of the solid PE [35]. Also drawn in Fig. 1 is the experimental heat capacity of the completely crystalline, extended-chain polyethylene, as it was determined earlier [36]. Fiber A shows a step-increase in heat capacity in the range from 260 to 290 K, relative to each of the Fiber B.

3.2. Melting behavior

The DSC data of the constrained UHMM-PE fibers is shown in Fig. 2(a). Measurements were made on six, short UHMM-PE filaments, which were placed parallel and tightly enclosed in a crimped sample pan. In these data we found double melting peaks at 415 and 423 K, with a total heat of fusion, $\Delta H_{f,total} (= \Delta H_{f,1} + \Delta Hf, 2)$ of 3.44 kJ mol^{-1}. Fig. 2(b) displays the DSC data of the unconstrained UHMM-PE fibers. In this run only a single, sharp endothermic peak was observed at 416 K with a $\Delta H_{f,total}$ of 3.54 kJ mol^{-1}, similar to that from the crimped fibers. The peak was sharp with a peak-width of about 2 K and was located close to the first endothermic peak observed under constraint. The sharpness of this transition may be because of a change in the superheating during the melting process. The first melting molecules add to the oriented, intermediate material and cannot relax fully, i.e. they have a higher melting temperature because of a smaller entropy of fusion. As soon as the constraint owing to the network of crystals is lost, however, the melting of the subsequent crystals goes immediately to a relaxed melt. If such a decrease in melting temperature during fusion is sufficiently large, it is known to even lead to a cooling of the sample, despite the heating supplied by the calorimeter [15,16]. In the present case, a sharpening of the melting peak beyond that expected from the crystal size distribution is seen in Fig. 2. It should be noted that the onset of melting occurs somewhat above the equilibrium melting point of extended chain polyethylene crystals given above (414.6 K). This is typical for highly drawn crystalline fibers.

To further study the origin of the double melting peaks seen in Fig. 2(a), experiments were performed on samples of various masses. In the prior experiments, the lower mass

Table 3
The transition parameters obtained in the melting region of UHMM-PE fiber III (ΔH_1 and ΔH_2 were estimated based on a Gaussian peak approximation)

Sample mass (mg)	$T_{m,1}$ (K)	$T_{m,2}$ (K)	ΔH_1 (kJ mol^{-1})	ΔH_2 (kJ mol^{-1})	ΔH_{total}(kJ mol^{-1})
0.025	415.2	423.5	1.40	2.24	3.64
0.053	415.6	423.3	1.77	1.77	3.54
1.146	416.8	425.7	2.45	0.86	3.31

alone seemed to eliminate the high-temperature melting peak [11,12]. Samples weighing between 25 μg and 1.15 mg were used. Assuming that the endothermic peaks have Gaussian profiles, transition parameters in the melting region have been determined and are listed in Table 3. All samples had double endothermic peaks in the temperature range between 410 and 435 K, in contrast to the earlier measurements that showed a single, sharp melting peak for masses of 24 μg and double peaks for masses 1.0 mg and higher. The locations of double endotherms remain practically constant for all masses, but the ratio of sizes of the two endotherms ($\Delta H_1/\Delta H_2$) varied with sample mass. The size of the lower endotherm is much larger for the 1.146 mg sample.

3.3. Wide-angle X-ray diffraction

Parallel to the DSC measurements, a series of equatorial and meridional X-ray diffractometer scans were made on bundles of restrained UHMM-PE fibers, as a function of temperature, by heating at a rate of about 1.0 K min^{-1}. Fig. 3 illustrates some typical results for the equatorial diffraction and Fig. 4 shows the meridional ones. The strong equatorial peaks at room temperature at $2\theta = 21.5$ and 23.5° correspond to the (110) and (200) lattice planes of the orthorhombic polymorph. The orthorhombic 110 peak has a half-width of approximately 0.5° (in 2θ), proving that the orthorhombic crystal phase is well ordered in the lateral direction. The constrained fibers in Fig. 3 are completely melted at about 419 K (Fig. 3(f)), and show at 415–418 K an increasing reflection at $2\theta = 20.5°$, the 100 diffraction peak position of the hexagonal polymorph.

The meridional diffractometer scans of the constrained UHMM-PE fibers in Fig. 4 show only one intense peak at $2\theta \approx 74.7°$, which corresponds to the (002) planes of the orthorhombic crystals. The increase of the position 002 of the peak in the temperature range of 415–418 K may be due to an increased gauche conformation of the chains at elevated temperatures. In addition, we also found an increased broadness of the 002 peak in the same temperature range. The intensity of the 002 peak decreases continually and disappears at approximately 418 K. In the meridional scan there was only a weak intensity at $2\theta = 74.9°$, indicative that the longitudinal order of the hexagonal crystal is not prominent, whereas a high degree of packing order can be found in the lateral direction, as seen in Fig. 3.

The magnified insert in Fig. 3 illustrates that at room temperature the usual amorphous background scattering is practically absent. The 110 peak can be seen to overlap with two very weak peaks at values of $2\theta = 19.5$ and 20.5°, which are the 010 and 100 diffraction peaks of the monoclinic and hexagonal crystals, respectively. The coexistence

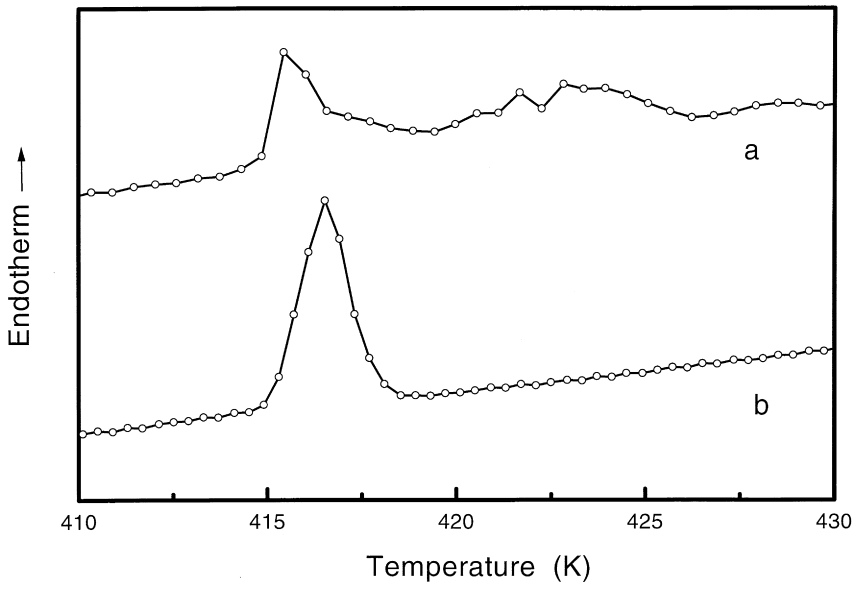

Fig. 2. Typical DSC heating scan of the UHMM-PE fibers using a 10 K min^{-1} scanning rate in the temperature range of 410–430 K. The curves are obtained from: (a) the constrained; and (b) the unconstrained fibers.

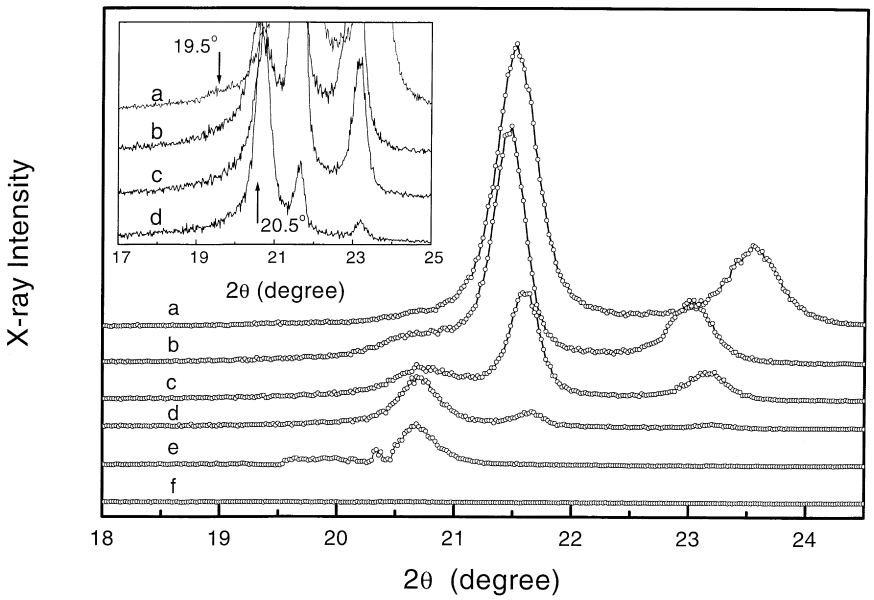

Fig. 3. Wide-angle equatorial X-ray diffractometer scans of the constrained UHMM-PE fibers recorded at: (a) 296 K; (b) 415 K; (c) 416 K; (d) 417 K; (e) 418 K; and (f) 419 K; during heating at about 1.0 K min^{-1}.

of these peaks indicates that the crystalline phase of the UHMM-PE fibers is polymorphic, but at low temperature, there are almost only orthorhombic crystals. On heating under constraint the hexagonal diffraction increases strongly in the melting region. The sharpness of the hexagonal peak shown in Fig. 3(d) and (e) indicates that the hexagonal crystal also possesses long-range order in the lateral direction. Above 418 K, it also starts disappearing, in parallel with the second melting peak.

The unconstrained fibers were analyzed earlier, using a two-dimensional full-pattern analysis and powder diffraction patterns using finely chopped fibers [9]. They melted completely without an increase in the hexagonal diffraction peak. The monoclinic fraction is small and disappears before melting of the orthorhombic phase, but increases in amount on lateral compression [9].

The positions of the orthorhombic 200 diffraction peaks vary with temperature, as is shown in Fig. 5 for both the constrained and unconstrained samples. Up to $\approx$ 415 K, the orthorhombic 200 peaks shift to a lower angle region by

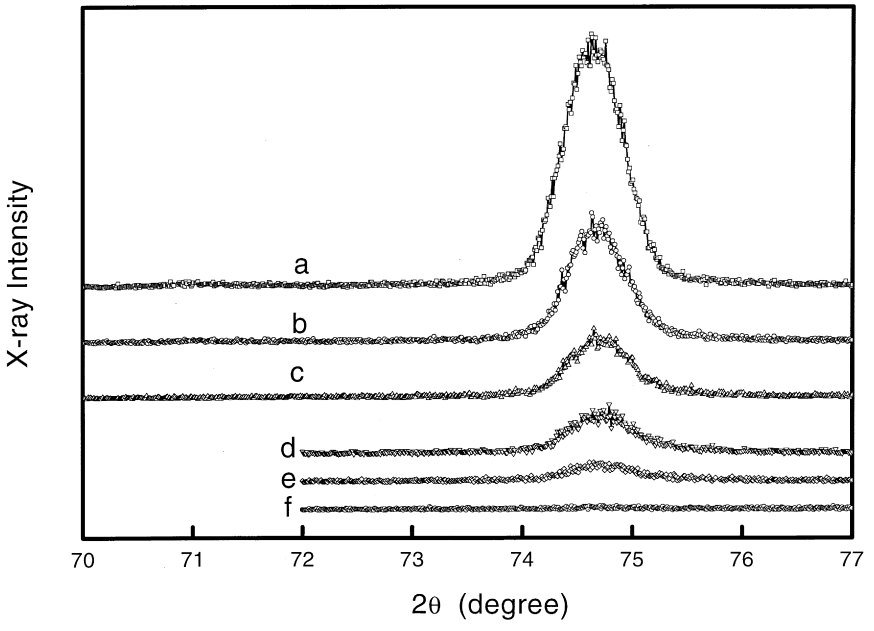

Fig. 4. Observed wide-angle meridional X-ray diffractometer scans of the constrained UHMM-PE fibers recorded during heating at about 1.0 K min^{-1}: (a) 296 K; (b) 377 K; (c) 402 K; (d) 411 K; (e) 415 K; and (f) 417 K.

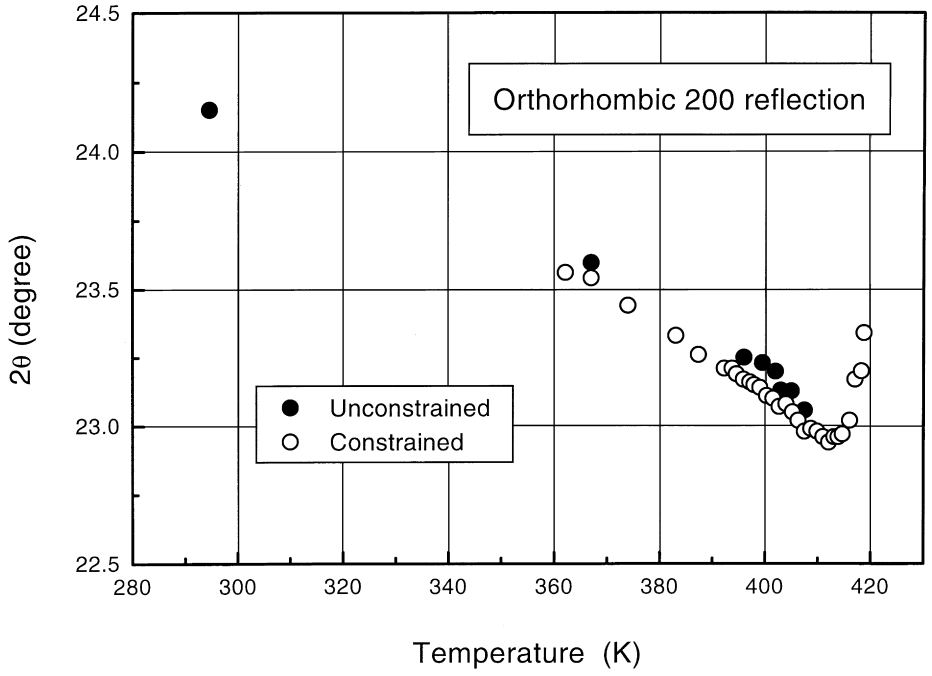

Fig. 5. Plot of the orthorhombic 200 diffraction peak with temperature for the constrained and unconstrained fibers.

approximately 1.0° per 100 K because of thermal expansion. Continuing the heating up to 418 K, the diffraction peak shifts back to the wider-angle region, probably because of crystal perfection, which parallels the shrinkage of the fibers on heating. The shrinkage behavior of the UHMM-PE fibers was confirmed using TMA at a heating rate of 10 K min^{-1}, hot stage microscopy with continuous heating rates of 2–5 K min^{-1}, as well as by the observation of a macroscopic fiber in a thermostated oil bath, where the temperature was increased in small steps of temperature [12].

Figs. 6 and 7 summarize the equatorial changes in d-spacings and intensities of the orthorhombic and hexagonal phases for the constrained fibers, respectively. Fig. 8(a) and (b) show the same changes for the meridional 002 reflection of the orthorhombic phase.

The approximate transverse crystallite sizes of the orthorhombic and hexagonal phases and can be assessed using the Scherrer equation. Assuming that the peak has a Gaussian profile, the integral half-widths of the peaks at $2\theta = 20.5$, 21.5 and 23.5° were established after correction for the instrumental broadening. Fig. 9 illustrates the changes of the transverse crystallite sizes of the orthorhombic and hexagonal crystals on heating. No significant change could be seen up to 415 K, when the first melting occurs. Between 415 and 418 K a slight increase occurs in the orthorhombic crystallite size because of annealing. The hexagonal crystals undergo a step-increase in width on their large increase in intensity (see Fig. 7), but do not reach the size of the orthorhombic crystals.

4. Discussion

4.1. Heat capacity

The heat capacity of any polymeric material is the basic information for the analysis of its state of molecular motion, phase transitions, degree of crystallinity and, thus, the temperature range of end-use. It is therefore surprising to find that there is no literature on the heat capacity of UHMM-PE fibers. This lack of information is because of the fact that when measuring fibers, errors of more than 10% are common when applying standard techniques. The problems of sufficient sample mass, non-reproducible settling of the sample inside the pan, shrinking and annealing effects and other variables frustrate any attempt in measuring the heat capacity with a reasonable degree of precision.

The use of multiple samples, measured on heating as well as cooling, and the use of several special preparation techniques did, however, lead in the present case to acceptable errors of the order of 1–3%. These values are comparable to commonly achieved precision in heat capacity measurements by DSC, but needed much preparatory work.

Fig. 1 illustrates the correlation of the heat capacity data of Table 2 with the literature information [35]. The post-stretch annealed samples (PE-I, II and III, called Fibers B) have close to identical heat capacities. Sample PE-IV (Fiber A), which is not post-stretch annealed, shows a step-wise increase in heat capacity Fibers B in the range from 260 to 290 K. Comparing the heat capacities to the experimentally determined heat capacity of a fully crystalline, extended-chain polyethylene [36] clarifies the changes on fiber

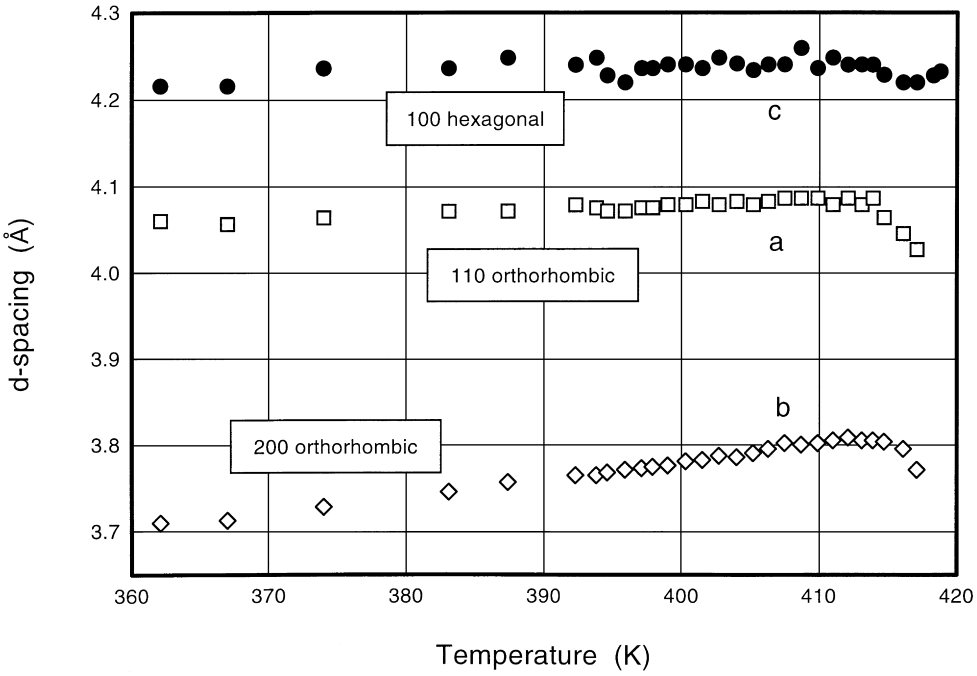

Fig. 6. Plot of the dependence of the *d*-spacings of peaks, for the constrained UHMM-PE fibers during heating: (a) 110 orthorhombic peak; (b) 200 orthorhombic peak; and (c) 100 hexagonal peak.

formation, and is shown in Fig. 10. The heat capacity of the fully crystalline material agrees up to about 250 K to the vibrations-only heat capacity calculation with the exception of a small anharmonicity effect (see Fig. 1) [35]. Above this temperature, the increasing amount of large-amplitude motion, linked to an increasing number of gauche conformations in the polyethylene chains increases the heat capacity of the fully crystalline, extended chain material [37]. The difference plot of Fig. 10 eliminates, thus, most of the heat capacity contribution of the orthorhombic crystals.

Fig. 10 delineates three distinct temperature regions. The first region, between 190 and 290 K, reflects a continuous increase in the heat capacity of the fibers over that of the extended-chain material. This temperature region coincides in its lower range (190–250 K) with the glass transition region of amorphous polyethylene, extrapolated from semicrystalline bulk polyethylene [38,39]. Fibers B reach an excess heat capacity beyond the vibrational heat capacity of about $3.0\,J\,K^{-1}\,mol^{-1}$, and Fiber A continues this increase to a final excess heat capacity of $4.4\,J\,K^{-1}\,mol^{-1}$.

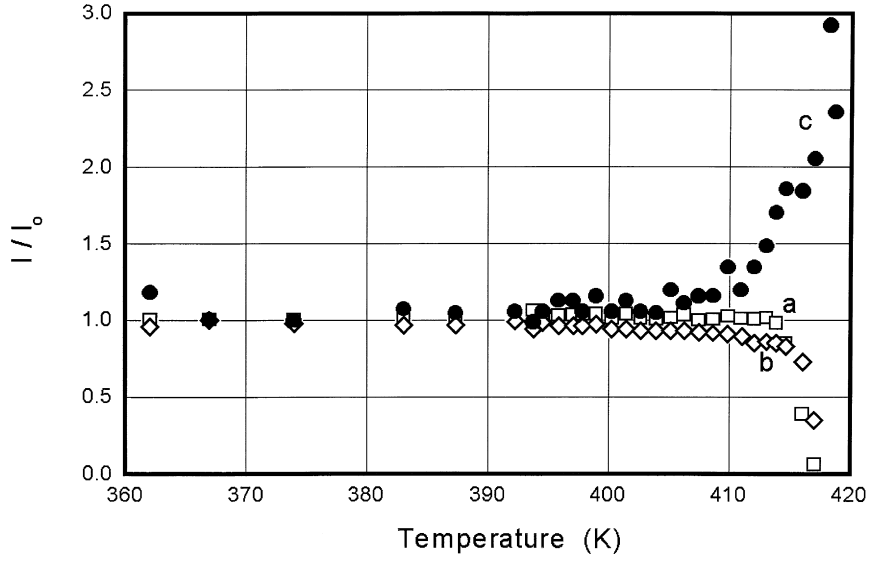

Fig. 7. The plot of the dependence of the intensities of the X-ray diffraction peaks for the constrained UHMM-PE fibers during heating relative to the intensity at low temperature (I_o): (a) 100 orthorhombic peak; (b) 200 orthorhombic peak; and (c) 100 hexagonal peak.

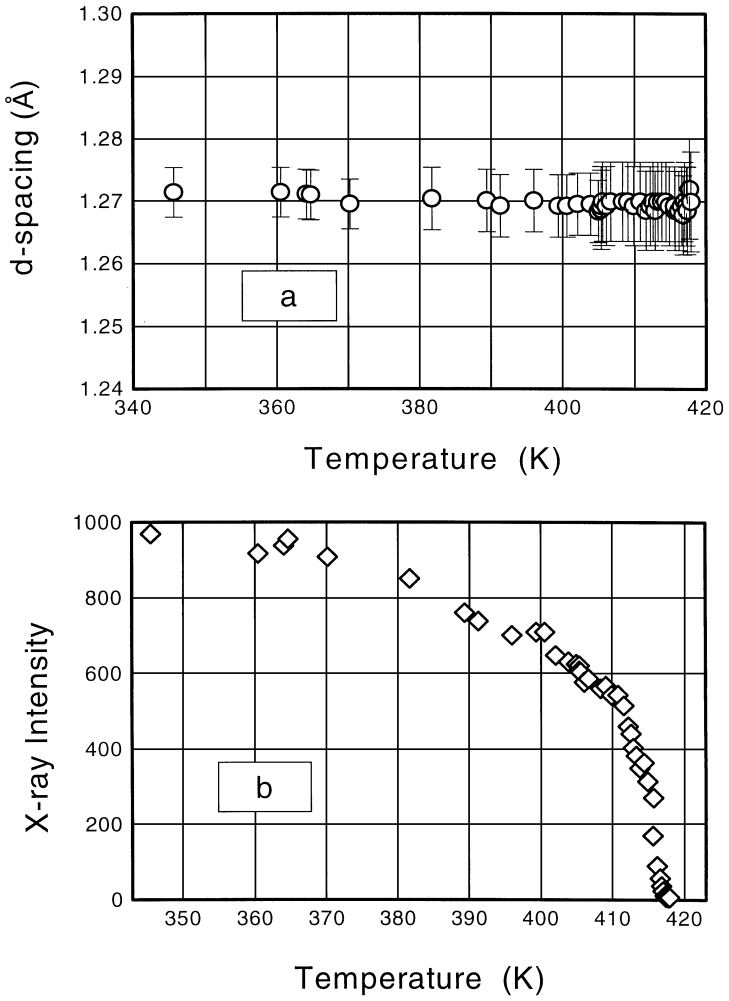

Fig. 8. Plot of the dependence of the *d*-spacing (a) and the intensity of the orthorhombic 002 peak for the constrained UHMM-PE fibers during heating.

By analogy to other semicrystalline polymers, the glass transition region is broadened to higher temperatures over that of the more amorphous material.

The increase in heat capacity of Fibers B and A would, however, correspond to an amorphous content of 33 and 48%, respectively, when using the recommended experimental heat capacities for amorphous and crystalline polyethylene at 300 K ($\Delta C_p = 9.08\ J\ K^{-1}\ mol^{-1}$) [40]. These amorphous contents do not agree with the calorimetric or volumetric crystallinities of Table 1, which are spread rather irregularly between 8–23% and 12–20%, respectively, and certainly they do not agree with the data on X-ray scattering seen in Fig. 3.

To resolve this problem, we consider the oriented, intermediate phase, proven earlier [9] to consist of chains with mobile, largely *trans*-conformations that are oriented parallel to the fiber axis, to also contribute to the glass transition to the same degree as the amorphous fraction. A similarity of the change in heat capacity at the glass transition in mesophases and amorphous polymers has been observed for several materials [41]. This mesophase can also contribute, in the case of well-annealed fibers, to the 00*l* X-ray reflections, but does not have the sufficient lateral order to contribute to the equatorial *hk*0 reflections in order to be considered a fully ordered crystal. From solid state ^{13}C NMR, PE-I was shown to have approximately 3% amorphous phase, while PE-IV has about 10% [9]. For this discussion we assume that the discrepancy between the calorimetric crystallinities of Table 1 and the amorphous fraction gained from the glass transition analysis is because of the remaining heat of fusion of the mesophase, rather than none, as was assumed in the prior discussions. For Fibers B and A, heats of fusion of the mesophases of 43 and 34% of the heat of fusion of the orthorhombic crystals ($4.11\ kJ\ mol^{-1}$), respectively, would make the crystallinity data to coincide. Such smaller heats of fusion are not unreasonable when compared to the hexagonal condis phase of polyethylene seen when heating the fibers under constraint (Figs. 3 and 7) or heating bulk polyethylene to elevated pressures [41]. The increase of order in the oriented intermediate phase on annealing (Fibers B) is also reasonable since this mesophase is assumed to be metastable, and its order is set by its mechanical and thermal history, not a global thermodynamic minimum in the

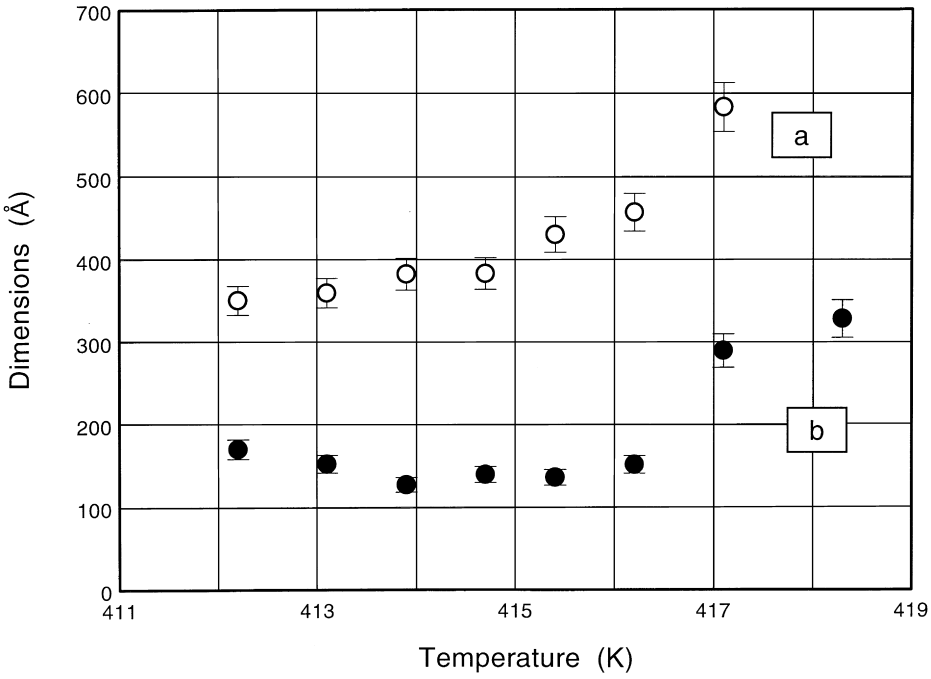

Fig. 9. Plot of the dependence of the transverse crystallite size of: (a) the orthorhombic; and (b) hexagonal crystal on temperature.

free energy. The so-corrected crystallinities are listed in brackets in Table 1.

The temperature range from 290 to 360 K is dominated by a plateau in the heat capacity for Fibers B and A. The existence of this plateau shows that the increase in heat capacity, owing to the increasing number of gauche conformations, occurs for Fibers B at about the same rate as in the fully crystalline, orthorhombic crystal phase of the extended-chain polyethylene, while a slight, additional increase exists for Fiber A. Again, this is a reasonable result if one considers that in the case of the unannealed fiber the oriented, intermediate phase has a lower heat of isotropization, i.e. it is already more disordered and can more easily increase further in disorder, an effect that is also commonly seen in liquid crystals.

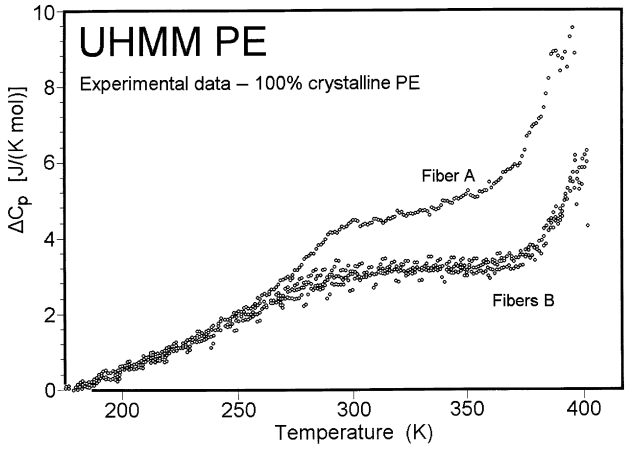

Fig. 10. Difference of the heat capacities of UHMM-PE fibers I, II and III (Fibers B) and of fiber IV (Fiber A) as presented in Table 2 to 100% crystalline, extended chain polyethylene (see also Fig. 1).

The final increase in heat capacity that leads into the melting peak begins for Fiber A at about 350 K, and for Fibers B at about 370 K. The heat capacities, being measured on heating and cooling without ultimately melting the samples, indicate that this second increase in heat capacity occurs also reversibly. Similar effects have been found recently for several semicrystalline bulk polymers when studied by temperature-modulated calorimetry [42–44]. This increase in heat capacity, which ultimately merges with the melting peak, was linked to the reversible melting of surface and intercrystalline material. One would assume the same to be true for the UHMM-PE fibers. The fact that the heat capacity of the Fiber A increases at lower temperature is in line with its unannealed character.

4.2. Melting behavior

The new standard DSC measurements of Fig. 2 and Table 3 clarify the origin of the double melting peak. The main effect is not directly because of the large sample mass, as suggested before [11], but is caused by the larger lateral constraint that is introduced with the increasing sample mass occupying a similar volume. Optical microscopy of the fibers during heating revealed a large lateral expansion as soon as shrinkage starts [12]. This means that the laterally constrained fibers behave similar to the fibers held at constant length. The environment of the fibers inside the pan is, thus, crucial in determining the melting behavior of the sample. Similar reasoning can be applied to the other observations of single melting peaks. As soon as

longitudinal and lateral restraints are removed, the higher melting peak disappears [21–24].

From the heat capacity measurements described above, it can be seen that the melting begins reversibly at 350–370 K, and it slowly becomes increasingly irreversible. A link of this with the X-ray intensities and crystal sizes will be given below. When the temperature exceeds about 415 K, at the sharp upturn lower temperature endotherm, major irreversible melting of the orthorhombic crystals occurs and if the sample is constrained, the hexagonal mesophase phase appears as the orthorhombic melting progresses.

Calorimetrically the polymorphism of the UHMM-PE is thus identified as follows: (1) The orthorhombic phase yields the major melting peak, at about 415 K, which is superheated by several degrees and varies in magnitude owing to the existing restraint on the sample; (2) the hexagonal phase that is generated by melting of the orthorhombic phase under external constraint gives rise to one or more endotherms between 420 and 430 K [22]; (3) calorimetry by itself cannot identify the melting of the small amount of monoclinic phase discovered by X-ray diffraction, but it was shown earlier, also by X-ray diffraction, that it disappears at a lower temperature than the orthorhombic phase [9]; (4) the intermediate oriented mesophase could be identified by the behavior in the glass transition region. Its presence is supported by the full-pattern X-ray data and the mobile *trans*-conformations, and identified by solid-state NMR [9]. (5) The truly amorphous phase can be judged only qualitatively from the sharpness of the glass transition region. It had to be separated by measuring the mobile gauche conformations by ^{13}NMR [9].

4.3. Wide-angle X-ray diffraction

The new wide-angle X-ray diffraction data on constrained and relaxed UHMM-PE fibers allows the addition of structural details to the calorimetry discussed above. Again, this discussion is a continuation of the earlier work on the same samples, which included full-pattern X-ray diffraction [9], SAXS [9], solid state ^{13}C NMR [10,13,14], DSC [11], TMA [12] and optical microscopy [9,12] as well as the large amount of prior knowledge reported in the literature [1–8].

At room temperature the X-ray data of Figs. 3 and 4 indicate that the main constituent of the sample is the orthorhombic crystalline phase. The small amount of the monoclinic, hexagonal and amorphous polymorphs are most likely inconsequential for the overall structure and properties of the fiber. The oriented intermediate phase cannot be detected easily from such diffraction patterns. Only by the full-pattern analysis could it be discovered for fiber PE-III that there is an extra component near the 002 reflection that does not agree with the overall intensities of the diffraction pattern of the orthorhombic crystal [9]. The more conclusive proof that there is a substantial amount of intermediate phase was brought by the ^{13}C NMR, the deficit in heat of fusion, density and now also the heat capacity. For practical applications, it is of importance to know the fraction and morphology of the oriented intermediate phases and their interaction with the orthorhombic and amorphous phases.

The time-resolved X-ray data, as presented in Figs. 5–9, permit some insight into the fiber structure, and the melting and transition behavior gives some understanding about the stability of the various polymorphs. With no external strain, it is obvious that no additional hexagonal phase is produced. The ordered-intermediate mesophase disappears along with the melting of the orthorhombic crystal. In fact, the single, sharp melting-peak, which agrees with the disappearance of the 002 X-ray diffraction as plotted in Fig. 8, agrees well with the calorimetry data. The reversible melting of Fibers B in Fig. 10 goes parallel with the first decrease in the diffraction-peak intensity in Fig. 8(b), while the melting peak at 415–417 K is in the center of the second, sharp decrease in intensity.

Up to about 415 K, the fiber repeat, *c*- (Fig. 8(a)), and the lateral *b*-dimension (Fig. 6(a)) of the orthorhombic crystal remain almost constant, while the *a*-dimension (Figs. 5 and 6(b)) gradually increases with temperature, accounting for practically all of the thermal expansion. This increase in the *a*-direction with temperature results in a gradual approach of the orthorhombic lattice to a hexagonal symmetry, which would be reached at a much higher temperature when $a = b$. In the same heating scan, the *a*-dimension of the hexagonal crystal remains almost constant up to 415 K (Fig. 6(c)).

Based on these data, the changes of the cross-sectional area in the orthorhombic and hexagonal crystals can be calculated, as shown in Fig. 11. For the constrained fibers, the area per chain in the hexagonal phase is approximately 20–25% larger than that for the orthorhombic crystal, as expected from its nature as a mesophase with increased mobility and conformational disorder [41]. In the temperature range of 415–418 K, one observes a decrease of the cross-section of both crystals, most likely connected to crystal perfection and melting of less perfect crystals, as can be judged from the increase in lateral crystal dimensions illustrated in Fig. 9. While the orthorhombic X-ray scattering peaks disappears over this temperature range, the hexagonal one increases rapidly in the case of fiber restraint, as seen in Fig. 7. As the amounts of hexagonal crystals increases at higher temperature, the cross-section of the chains again increases slightly (Figs. 6 and 11), an observation in line with the now constant lateral crystal dimension of Fig. 9.

The orthorhombic fiber repeat, *c*, shown in Fig. 8(a), decreases over the whole temperature range of measurement by about 0.05 Å, an effect that can be connected to the increased concentration of gauche-conformation mirrored in the gradual increase in the heat capacity (Fig. 1, curve for 100% crystalline PE).

The hexagonal mesophase in UHMM-PE fibers, when analyzed under highly restrictive external forces, have been observed earlier [1,22,45–47]. The chains in this mesophase phase possess some degree of mobility, but

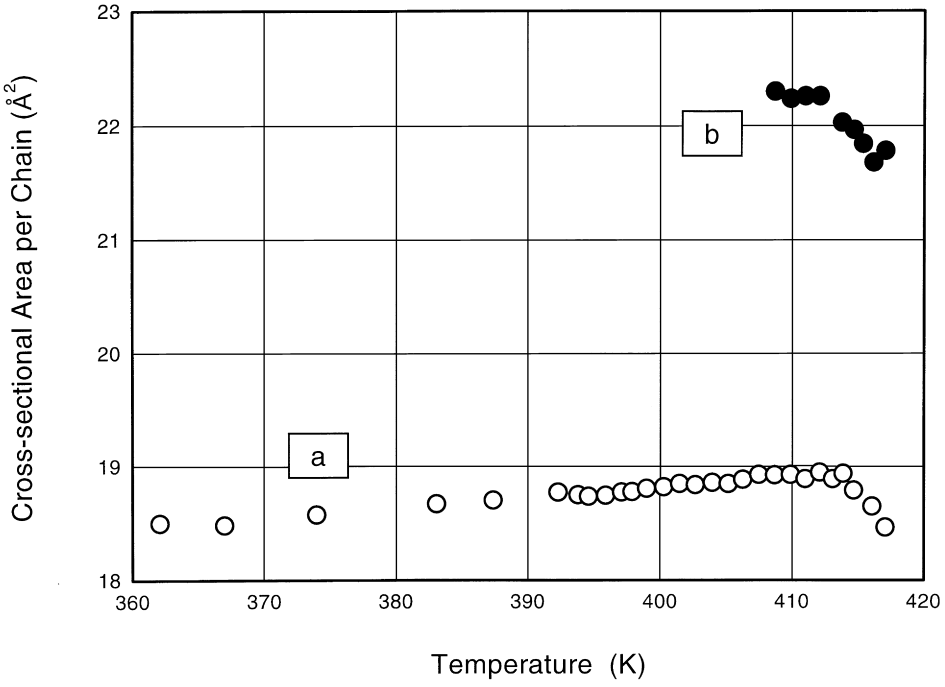

Fig. 11. Plot of the dependence of the cross-sectional area per chains in: (a) the orthorhombic; and (b) hexagonal phases.

with a longer-range order in the lateral direction than in the intermediate oriented mesophase. The weakness and broadness of the meridional X-ray peak of the hexagonal mesophase indicates, that the axial correlation between neighboring chains is low, because of the high mobility and large number of defects.

5. Conclusions

The crystalline phase of the UHMM-PE fibers is polymorphic. It consists of mainly orthorhombic crystals and an oriented intermediate phase. The oriented mesophase is kept in its metastable state by the orthorhombic crystals, but governs much of the mechanical properties [9]. Small amounts of monoclinic, hexagonal and amorphous phases round out the total composition. These three phases have little influence on the properties of the fibers as long as their concentration remains small.

The double-melting peak on analysis by DSC is only found for longitudinally or laterally constrained fibers. Under such constraints, larger amounts of the hexagonal phase form. Since the hexagonal phase is not stable at atmospheric pressure without restraint, it seems to be stabilized together with the oriented intermediate phase by the external constraint.

Removing the constraint, the fibers melt with a sharp single melting peak. As soon as the orthorhombic crystals melt, the oriented intermediate phase becomes unstable and melts together with the orthorhombic crystals, but with less than half the heat of fusion of the orthorhombic crystals. The melting temperature of the fibers is elevated above the equilibrium melting temperature of orthorhombic polyethylene because of the initial presence of the oriented intermediate phase to which the melting crystal chains could add only with a lower entropy of fusion and with a higher melting temperature [16]. A more detailed explanation of single and multiple melting peaks of UHMM-PE is, thus, possible.

From the calorimetry of the fibers we could derive, besides the melting characteristics, extensive heat capacity information. The heat capacity allowed the identification of the broadened glass transition of the oriented intermediate phase, establish better estimates of the amount of the intermediate phase and document a small amount of reversible melting at lower temperature than the major irreversible melting.

The combination of X-ray structure analysis, detection of molecular motion by NMR and macroscopic thermal analysis (DCS, TMA, dilatometry and optical microscopy) allowed a more detailed analysis of the gel-spun UHMM-PE fibers. The interpretation of all the measurements done on this set of identical fibers points to further advances by: (A) quantitative analyses, of the type similar to that carried out in this research, on broader ranges of samples of different thermal and mechanical history; and (B) application of new techniques, such as for example the temperature-modulated DSC, in order to delineate the reversible and irreversible processes on annealing and melting, as done recently with linear low density polyethylene [42].

Acknowledgements

This work was supported by the Division of Materials Research of National Science Foundation, Polymer Program, Grant No. DMR-9703692 and Division of Materials Science of the Office of Basic Energy Sciences, DOE at Oak Ridge National Laboratory, managed by Lockheed Martin Energy Research Corp. for DOE, under contract number DE-AC05-96OR22464.

References

[1] Clough SB. Polym Lett 1970;8:519.
[2] Gibson AG, Davies GR, Ward IM. Polymer 1978;16:683.
[3] Pennings AJ. J Polym Sci, Polym Phys Ed 1979;17:1011.
[4] Smith P, Lemstra PJ. J Mater Sci 1980;15:505.
[5] Grubb DT, Prasad K. Macromolecules 1992;25:4575.
[6] Hofmann D, Schulz E. Polymer 1989;30:1964.
[7] Saraf AW, Desai P, Abhiraman AS. J. Appl Polym Sci, Polym Symp 1991;47:67.
[8] Moonen JHAM, Roovers WAC, Meier RJ, Kip BJ. J Polym Sci, Polym Phys Ed 1992;30:361.
[9] Fu Y, Chen W, Pyda M, Londono JD, Annis B, Boller A, Habenshcuss A, Cheng J, Wunderlich B. J Macromol Sci Phys B 1996;35:37.
[10] Chen W, Fu Y, Wunderlich B, Cheng J. J Polym Sci, Polym Phys Ed 1994;32:2991.
[11] Boller A, Wunderlich B. J Thermal Anal 1997;49:343.
[12] Boller A. The thermal analysis of gel-spun ultra-high molar mass polyethylene fibers. Thesis, University of Tennessee, Knoxville, 1966.
[13] Cheng J, Fone M, Fu Y, Chen W. J Thermal Anal 1996;47:673.
[14] Cheng J, Fone M, Reddy VN, Schwartz KB, Fisher HP, Wunderlich B. J Polym Sci, Polym Phys 1994;32:2683.
[15] Wunderlich B. Thermal analysis of materials. A computer-assisted lecture course, published on the Internet (web.utk.edu/athas/courses/tham99.html) downloadable including presentation software 1998/1999.
[16] Wunderlich B. Crystal melting, Macromolecular physics, 3. New York: Academic Press, 1980.
[17] Wunderlich B. Crystal structure, morphology, defects, Macromolecular physics, 1. New York: Academic Press, 1973.
[18] Arakawa T, Wunderlich B. J Polym Sci C 1967;16:653.
[19] Atkinson CML, Richardson MJ. Trans Farad Soc 1969;65:1749.
[20] Wunderlich B, Czornyj G. Macromolecules 1977;10:906.
[21] Murthy NS, Correale ST, Kavesh S. Polym Commun 1990;31:50.
[22] Pennings AJ, Zwijnenburg A. J Polym Sci, Polym Phys Ed 1979;17:1011.
[23] Economy J, Andreopoulos AG. Polym Adv Tech 1994;5:349.
[24] Batiaansen CWM, Lemstra PJ. Makromol Chem, Makromol Symp 1989;28:73.
[25] Todoki M, Kawaguchi T. J Polym Sci, Polym Phys Ed 1977;15:1067.
[26] Wunderlich B. Crystal nucleation, growth, annealing, Macromolecular physics, 2. New York: Academic Press, 1976.
[27] Höhne GWH, Glöggler E. Thermochim Acta 1989;151:295.
[28] Höhne GWH, Schawe JEK. Thermochim Acta 1993;229:27.
[29] Smith P, Lemstra PJ, Pennings AJ. German Patent 30 04 699, 1980.
[30] Smith P, Lemstra PJ. US Patent 4 422 993, 1983.
[31] Kavesh S, Prevorsek D. US Patent 4 413 110, 1983.
[32] Boller A, Ribeiro M, Wunderlich B. J Therm Anal Calorim 1998;54:545.
[33] Wunderlich B. Thermal analysis. Boston: Academic Press, 1990.
[34] Statton WO, Godard GM. J Appl Phys 1957;22:191.
[35] Wunderlich B. The ATHAS data base of heat capacities of polymers. Pure Appl Chem 1995;67:1919 see also our internet-site at web.utk.edu/~athas .
[36] Wunderlich B. J Phys Chem 1965;69:2078.
[37] Sumpter BG, Noid DW, Liang GL, Wunderlich B. Atomistic dynamics of macromolecular crystals. Adv Polym Sci 1994;116:27.
[38] Gaur U, Wunderlich B. Macromolecules 1980;13:445.
[39] Wunderlich B. J Chem Phys 1962;37:2429.
[40] Gaur U, Wunderlich B. J Phys Chem 1981;10:119.
[41] Wunderlich B, Möller M, Grebowicz J, Baur H. Conformational motion and disorder in low and high molecular mass crystals, Advances in polymer science, 87. Berlin: Springer, 1988.
[42] Androsch R, Wunderlich B. Macromolecules 1999;32:7238.
[43] Ishikiriyama K, Wunderlich B. Macromolecules 1997;30:4126.
[44] Okazaki I, Wunderlich B. Macromolecules 1997;30:1758.
[45] Bassett DC, Block S, Piermarini G. J Appl Phys 1974;45:4146.
[46] Yasuniva M, Nakafuku C, Takemura T. Polym J 1974;4:526.
[47] Ungar G, Keller A. Polymer 1980;21:1273.